Progress of Theoretical Physics, Vol. 64, No. 6, December 1980

Dissipation of the Primordial Terrestrial Atmosphere Due to Irradiation of the Solar EUV

Minoru SEKIYA, Kiyoshi NAKAZAWA and Chushiro HAYASHI

Department of Physics, Kyoto University, Kyoto 606

(Received August 11, 1980)

The escape of a primordial Earth's atmosphere due to heating by solar radiation is studied by integrating numerically hydrodynamic equations for steady and spherically-symmetric outflow of hydrogen molecules and helium atoms. As heating sources, we take account of (1) the solar EUV radiation which is expected to be very strong during the T Tauri stage, (2) the solar visible light and (3) the release of gravitational energy of accreting planetesimals. The effect of solar wind is neglected but the condition of this neglect is estimated.

The results show that the primordial atmosphere, having existed in the early stage of the Earth's history, is dissipated within a period of 5×10^8 y, which is the upper limit imposed from the origin of the present terrestrial atmosphere, as far as the solar EUV flux is more than 2×10^2 times as large as the present one.

§ 1. Introduction

The origin of the Earth's atmosphere is one of the most important problems for the theory of planetary formation in a sense that the theory can be tested by direct comparison with observations. It is well known that light rare gases are extremely depleted in the present atmosphere compared with those in the solar atmosphere. This indicates, as was first pointed out by Brown,[1] that the present atmosphere was not formed of gases of the primordial solar nebula. It is now believed that the gases of the present atmosphere had outgassed from the terrestrial interior within a period of less than 5×10^8 y after the Earth just grew to the present mass.[2),3]

On the other hand, the theory of planetary formation developed by Hayashi et al.[4),5),6] shows that the gas of the solar nebula played a very important role in various processes of planetary formation, such as in the growth of protoplanets through the accretion of planetesimals and also in the formation of the present giant planets as a result of gravitational instability of surrounding gases. It was also shown by Hayashi et al.[7),8] that when the Earth just grew to the present mass ($=6\times10^{27}$ g) it was surrounded by a hot and dense atmosphere with mass as large as 1×10^{26} g. Then, there arises a question how this primordial atmosphere could be dissipated into outer space before the formation of the present atmosphere, i.e., within the above-mentioned period 5×10^8 y.

We consider for this question that, first, the solar nebula was dissipated

gradually by the irradiation of the solar wind and UV radiation which are expected to be much stronger in the past T Tauri stage than at present and, subsequently, the primordial atmosphere was dissipated by direct UV irradiation from the sun. Recent observations of a T Tauri star, RU Lupi by Gahm et al.[9] indicate that the far-UV intensity in the wavelength between 1250Å and 1350Å is about $10^{4\sim5}$ times as strong as the present sun.

So far, the escape of the primordial atmosphere was studied by Gross,[10] Hunten[11] and Horedt.[12] Gross estimated the exospheric temperature under a simple assumption that the atmosphere is in hydrostatic equilibrium and a half of the solar EUV radiation is converted into heat at the exosphere and transfered steadily through conduction to the lower atmosphere where the heat is lost by infrared emission. He obtained, in the case of the Earth, the exospheric temperature as high as 1.5×10^4 K. This means that the atmosphere escapes very rapidly and, then, cannot be static. Therefore, the static thermal equilibrium model of Gross is too much simplified. On the other hand, Hunten estimated the mass loss of the primordial Martian atmosphere, assuming that all the energy of the solar visible light which irradiates Mars is available for the escape of the atmosphere. As seen later, however, almost all of the energy of the solar visible light absorbed by grain particles is re-emitted into outer space without any contribution to the mass loss. Recently, Horedt[12] calculated the mass loss of the primordial atmospheres of all the planets. He considered the solar EUV radiation and the solar wind as energy sources. He made a calculation of the mass loss on the assumption that the whole atmosphere is represented by a polytropic model. His treatment seems, however, to be too simple to obtain quantitative results. For example, according to our results (see Figs. 2 and 3), the polytropic index, $d\ln\rho/d\ln T$, varies greatly in the atmosphere and even takes negative values in the outer regions.

In the present paper, we calculate more precisely the mass loss of the primordial terrestrial atmosphere due to the irradiation of solar EUV. In § 2, we describe assumptions, heating and cooling processes and numerical procedures to solve hydrodynamic equations. In § 3, we show numerical results, discuss the dependence of the mass loss rate on various parameters and confirm the assumptions. Finally, in § 4, the results are summarized and also the dissipation time of the solar nebula is estimated.

§ 2. Basic equations and numerical procedures

We shall calculate the steady outflow of the atmosphere which is heated by three kinds of sources, (1) the solar EUV radiation absorbed in the upper atmosphere, (2) the solar visible radiation absorbed near the photosphere and (3) the release of energy of accreting planetesimals at the bottom of the atmosphere, as shown in Fig. 1. The last energy source is important only in regions inside the photosphere and it has a role only to increase the radius of the photosphere.

The solar visible light is absorbed mainly by dust grains existing in regions near the photosphere and is converted into infrared radiation which can escape almost freely into outer space. Owing to this energy source, however, the gas temperature near the photosphere is kept nearly constant. The solar EUV radiation is absorbed through ionization of H_2 molecules in the outer layers where the gas is heated up and accelerated outwards. This is the direct cause of the mass loss and the other sources aid the mass loss by increasing the radius (i.e., the gravitational energy) of EUV-absorbing layers in the Earth's gravitational field.

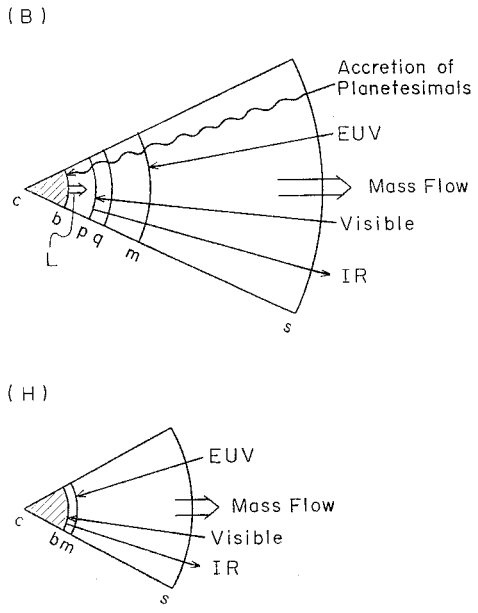

Fig. 1. The structure of the primordial atmosphere at an early and a late stage, as represented by the models (B) and (H) in Table I, respectively. The center of the Earth is denoted by *c*, the bottom of the atmosphere by *b*, the photosphere by *p*, the interface where a static solution is fitted to a steady flow solution by *q*, the minimum temperature point by *m* and the sonic point by *s*. In the model (H), the photosphere has disappeared and the solar visible light irradiates directly the surface of the Earth. The solar EUV flux is absorbed mainly in regions outside the point *m*. Almost all the energy of visible light absorbed near the photosphere is re-emitted as IR radiation and useless for the escape of the atmosphere.

Heating due to absorption of the solar far-UV radiation by water (H_2O) molecules will be important in view of the observations of RU Lupi as mentioned in § 1, but this heating is neglected in this paper for simplicity and will be studied in the next paper.[13] We also neglect heating due to solar wind as well as cooling due to thermal conduction and line emission from oxygen atoms. All of these will be examined and justified later in § 3. Moreover, we treat the whole problem in the approximation of spherical symmetry, in view of the terrestrial rapid rotation which smooths out the day and night difference in the flux of the solar radiation penetrating into the atmosphere.

We assume that the outflow of the atmosphere is steady. This assumption will be justified later in § 3.4(b). Now, flow velocity in the inner region is very small because, as we go inwards, the gas density increases very rapidly. Then, we divide the atmosphere into two regions, i.e., the inner and the outer atmospheres in such a way that the structure of the inner atmosphere is well approximated by

that of a static atmosphere (see § 2.4 for the determination of the interface). Recently, Nakazawa et al.[14] tabulated a wide variety of static solutions of the primordial Earth's atmosphere surrounded by a nebular gas with arbitrary density. We use these solutions for the inner atmosphere. Hereafter, we concentrate on the heating and motion of the outer atmosphere.

2.1. *Heating and cooling rates*

Before introducing equations governing the gas flow, we study here heating and cooling of gas molecules and dust grains in the outer atmosphere. We have three sources for gas heating, i.e., solar EUV radiation, solar visible radiation and infrared radiation coming from the photosphere outwards. The latter two sources cannot heat the gas directly but only heat grains, the gas being heated indirectly through collisions with grains.

The rate of gas heating by the solar EUV radiation per unit volume and time is given by

$$\Gamma_{\rm EUV}=F_{\rm EUV}\varepsilon\kappa_{\rm EUV}\rho\exp[-\tau_{\rm EUV}]/(1+a\tau_{\rm EUV}), \tag{2·1}$$

where ρ is the gas density, and $\kappa_{\rm EUV}$ and $\tau_{\rm EUV}$ are the opacity and the optical depth for the EUV radiation, respectively. Strictly speaking, $\kappa_{\rm EUV}$ depends on the wavelength of the radiation,[15] but we assume for simplicity that it is constant and equal to $9\times10^5\,{\rm cm^2\,g^{-1}}$. In this case, we have

$$\tau_{\rm EUV}=\kappa_{\rm EUV}\int_r^\infty\rho dr\,. \tag{2·2}$$

Furthermore, ε is the heating efficiency of the EUV radiation (which is about 0.42 as estimated in Appendix A) and $F_{\rm EUV}$ is the energy flux of the EUV radiation in the T Tauri stage. Unfortunately, the value of $F_{\rm EUV}$ is not well known at present and, hence, we regard $F_{\rm EUV}\varepsilon$ as a parameter. The denominator, $1+a\tau_{\rm EUV}$, in Eq. (2·1) represents the geometrical factor coming from the assumptions that the atmosphere is spherically symmetric and rotating rapidly (see Appendix B). The value of 'a' depends weakly on the shape of density distribution and we put simply $a=2$ in the following.

As is well known, the rate of gas heating through collisions with dust grains is given by

$$\Gamma_{\rm d}=(n_{\rm H_2}v_{\rm H_2}+n_{\rm He}v_{\rm He})n_{\rm d}\sigma_{\rm d}k(T_{\rm d}-T), \tag{2·3}$$

where n and v are the number density and the thermal velocity, respectively, and the subscripts H_2, He and d denote hydrogen molecules, helium atoms and dust grains, respectively. Furthermore, $\sigma_{\rm d}$ is the geometrical cross section of a grain, which is assumed to have a radius of 1 μm, and k, $T_{\rm d}$ and T are the Boltzmann constant, the grain temperature and the gas temperature, respectively. The grain number density $n_{\rm d}$ is related to the grain opacity, κ_g. Here we use the following

formula obtained by us from the table by Allexander et al.,[16] i.e.,

$$n_d = 86\kappa_g\rho/\sigma_d. \quad \text{(in c.g.s. units)} \tag{2·4}$$

As to gas cooling, line emission from oxygen atoms seems to be important. However, we have found that this cooling can be neglected compared with Γ_{EUV} and Γ_d (see § 3.4(e)). Then, the total net rate of gas heating is given by

$$\Gamma = \Gamma_{EUV} + \Gamma_d . \tag{2·5}$$

It is to be noticed that in order to know completely the value of Γ_d, we have to find the dust temperature T_d appearing in Eq. (2·3).

As is well known, the dust temperature is determined by a balance between the heating and cooling of grains, which is expressed as

$$\Gamma_V + \Gamma_{IR} = \Lambda_{IR} + \Lambda_{ex} , \tag{2·6}$$

where Γ_V is the rate of grain heating (per unit volume and time) due to absorption of solar visible radiation and Γ_{IR} is that due to absorption of infrared radiation coming from the photosphere. Further, Λ_{IR} is the rate of grain cooling due to infrared emission from the grain surface and Λ_{ex} is that due to energy exchange between the gas and the grains which is, of course, equal to Γ_d given by Eq. (2·3).

Expressions for Γ_V, Γ_{IR} and Λ_{IR} will be given in the following. First, Γ_V is expressed in the form

$$\Gamma_V = \kappa_g\rho F_V\delta . \tag{2·7}$$

Here, F_V is the energy flux of the solar visible radiation which is assumed to be equal to the present solar value ($=1.36\times10^6$ ergs cm^{-2} s^{-1}) and δ represents the shadow effect of the photosphere[7] which is given by

$$\delta = [1 + (1 - r_p^2/r^2)^{1/2}]/2 , \tag{2·8}$$

where r_p and r are the radii of the photosphere and the point under consideration, respectively. Second, Γ_{IR} is given by

$$\Gamma_{IR} = \kappa_g\rho\pi r_p^2 F_V/4\pi r^2\delta , \tag{2·9}$$

where we have assumed that the visible light irradiating the photosphere is completely re-emitted outwards as infrared radiation and also we have neglected the luminosity due to accreting planetesimals since this is much smaller than $\pi r_p^2 F_V$ and important only in regions inside the photosphere (see Fig. 1). Finally, Λ_{IR} is given by

$$\Lambda_{IR} = 4\kappa_g\rho\sigma T_d^4 , \tag{2·10}$$

where σ is the Stefen-Boltzmann constant.

2.2. *Equations of outflow in the outer atmosphere*

The spherical and steady outflow of the atmosphere is described by the equations of conservation of mass, momentum and energy, respectively, i.e.,

$$\rho u r^2 = \text{const} = |\dot{M}_g|/4\pi\,, \tag{2·11}$$

$$u\frac{du}{dr} = -\frac{1}{\rho}\frac{dP}{dr} - \frac{GM}{r^2}\,, \tag{2·12}$$

$$\rho u T ds/dr = \Gamma\,, \tag{2·13}$$

where u is the radial flow velocity, $|\dot{M}_g|$ is the rate of mass loss of the atmosphere, G is the gravitational constant, M is the Earth's mass, s is the specific entropy, P is the pressure and Γ is the heating rate given by Eq. (2·5). Assuming an ideal gas with an adiabatic exponent $\gamma(=1.43)$, we have

$$s = (k/\mu m_{\rm H})\ \ln\ [T^{\gamma/(\gamma-1)}/\rho], \tag{2·14}$$

$$P = k\rho T/\mu m_{\rm H}\,, \tag{2·15}$$

where $\mu(=2.34)$ and $m_{\rm H}$ are the mean molecular weight of the gas and the mass of a hydrogen atom, respectively. Although the mean molecular weight and the adiabatic exponent change with the dissociation of the hydrogen molecules, we neglect their change for simplicity. Instead of Eq. (2·13), we can also use the equation

$$\rho u dH/dr = \Gamma\,, \tag{2·16}$$

where H is a sum of the specific enthalpy and the gravitational energy, i.e.,

$$H = \frac{u^2}{2} + \frac{\gamma}{\gamma-1}\frac{P}{\rho} - \frac{GM}{r}\,. \tag{2·17}$$

2.3. *Structure of the inner atmosphere*

As mentioned earlier in this section, the inner atmosphere is well described by a hydrostatic model of the primordial atmosphere. If the Earth's mass is fixed to the present value and the energy outflow (i.e., the luminosity) in the atmosphere is assumed to be constant, the atmospheric structure is determined, as shown by Nakazawa et al.,[14] uniquely by four parameters, i.e., the density $\rho_{\rm H}$, the temperature $T_{\rm H}$ at the Hill surface (i.e., at $r=235\ R_{\rm E}$ where $R_{\rm E}$ is the Earth's radius), the mass accretion rate $\dot{M}$ (or the luminosity $L=GM\dot{M}/R_{\rm E}$ arising from the release of accretion energy at $r=R_{\rm E}$) and the grain opacity κ_g.

The former two parameters come from the outermost boundary condition, i.e., from the fitting of the atmospheric gas to the nebular gas. In regions between the Hill surface and the photosphere, the gas temperature is maintained nearly at 280 K. Hence, the atmospheric structure (including the atmospheric mass M_g) is

determined by one parameter ρ_H, if $\dot{M}$ and κ_g are both given. In other words, the structure is determined uniquely if $\dot{M}$, κ_g and M_g are all given.

2.4. *Boundary conditions and numerical procedures*

The interface between the inner and the outer atmospheres is set at a surface $r=r_q$ where the flow velocity is very small compared with the sound velocity and also the temperature gradient, $|d\ln T/d\ln r|$, is much smaller than unity. In this case, the inner atmosphere is represented well by a static model.

Numerical procedures are as follows. At first, we choose a set of values of κ_g, M_g and $\dot{M}$. Using a corresponding static solution, we find the density ρ_q at the interface. Then, with ρ_q, T_q (which is nearly equal to 280 K) and a trial value of the flow velocity, u_q, at the interface, Eqs. (2·11), (2·12) and (2·13) are integrated numerically outwards. Here, a boundary condition that a solution must go through a sonic point is required since, in the absence of the nebular gas, no external pressure is acting and the atmosphere can expand freely into outer space (the validity of this boundary condition in the presence of the solar wind will be examined in § 3.4(g)).

If a solution obtained for a trial value of u_q does not satisfy the above sonic point condition, another trial is made with a different value of u_q. This is continued until the condition is satisfied with sufficient accuracy. One more iteration is required before we obtain a final solution since it must satisfy a condition that, after passing through the sonic point, τ_{EUV} tends to zero as $r\to\infty$. For this, we set a trial value of τ_{EUV} at the interface, $r=r_q$, and integrate Eqs. (2·11) to (2·13) outwards. If τ_{EUV} does not come close to zero at a point where ρ is sufficiently low, the integration is repeated with another trial value of τ_{EUV} at $r=r_q$.

§ 3. Numerical results and discussion

The rate of mass loss of the primordial atmosphere depends, in a complicated manner, on the adopted parameters, i.e., the effective solar EUV flux εF_{EUV}, the grain opacity κ_g, the mass accretion rate $\dot{M}$ and the atmospheric mass M_g. The detail of the dependence on M_g will be described in § 4 and here we discuss mainly the dependence on εF_{EUV}, κ_g and $\dot{M}$. For this purpose, we have selected eight representative models, as listed in Table I, where the model (B) is to be considered as standard in a sense that all the other seven models are to be compared with it.

Here, we describe the ranges of the parameters adopted in all of our computations. First, εF_{EUV} ranges from 1 to 1×10^4 erg cm^{-2} s^{-1}, i.e., from 1 to 10^4 times the present solar EUV flux at 1 AU (note that $\varepsilon=0.42$). Second, the range of κ_g is from 0 to 1×10^{-2} cm^2 g^{-1}; κ_g is about 1 cm^2 g^{-1} in interstellar clouds but most of grains sedimented in early stages of the solar nebula and only a very small amount of grains, probably with $\kappa_g=10^{-4}\sim10^{-5}$ cm^2 g^{-1}, were floating at the time of planetary formation. Third, $M/\dot{M}$ is in the range $1\times10^9\sim1\times10^{10}$ y; when the

Earth was growing actively, $M/\dot{M}$ is about 1×10^6 y[5] but when it grew to the present mass, $M/\dot{M}$ was probably of the order of 10^9 y.

Table I. Parameters and mass loss rate of representative models. The model (H) is independent of mass accretion rate as far as $M/\dot{M}\gg10^8$ y, i.e., as far as the corresponding luminosity is much smaller than the total flux of the solar visible light which irradiates the Earth. Mass loss rate is given in the last column.

Model	M_g (g)	$M/\dot{M}$ (y)	κ_g (cm^2g^{-1})	εF_{EUV} ($erg\ cm^{-2}s^{-1}$)	$\lvert\dot{M}_g\rvert$ ($g\ y^{-1}$)
(A)	3.3×10^{25}	1×10^9	1×10^{-4}	1000	4.5×10^{17}
(B)	3.3×10^{25}	1×10^9	1×10^{-4}	100	1.6×10^{17}
(C)	3.3×10^{25}	1×10^9	1×10^{-4}	10	4.4×10^{16}
(D)	3.3×10^{25}	1×10^9	1×10^{-4}	1	7.8×10^{15}
(E)	3.3×10^{25}	1×10^9	1×10^{-2}	100	3.3×10^{17}
(F)	3.3×10^{25}	1×10^9	0	100	7.7×10^{16}
(G)	3.3×10^{25}	1×10^{10}	1×10^{-4}	100	1.1×10^{17}
(H)	1×10^{19}	—	1×10^{-4}	100	2.5×10^{16}

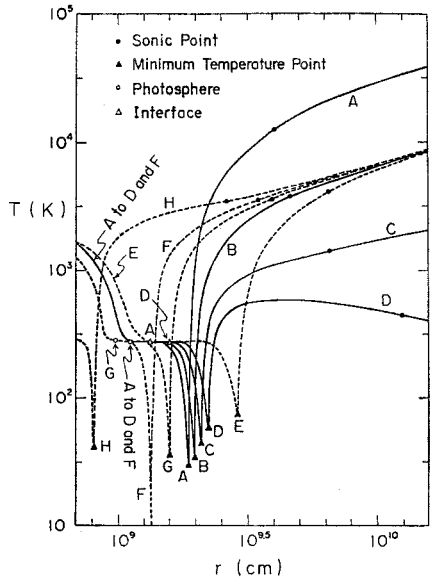

Fig. 2. The temperature distribution of the primordial atmosphere for the models (A) to (H) in Table I. The photosphere (i.e., the point p in Fig. 1) is denoted by the open circle, interface (the point q) by the open triangle, the minimum temperature point (the point m) by the closed triangle and the sonic point (the point s) by the closed circle.

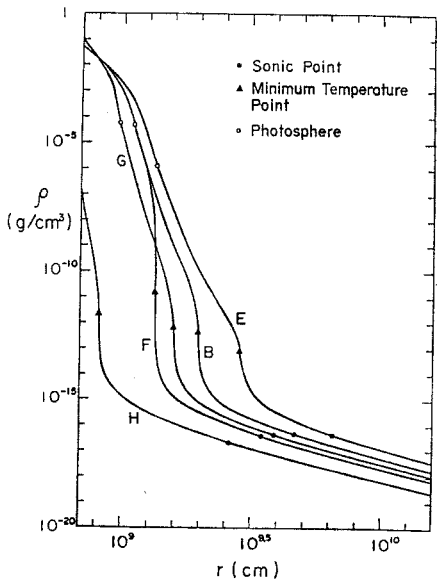

Fig. 3. The density distribution. The symbols are the same as in Fig. 2.

3.1. *General features of the models*

Before discussing the dependence of the mass loss rate on the parameters, we describe in this section the general features of all the models. As seen in Fig. 2, in the neighborhood of the interface between the inner and outer atmospheres (as denoted by the open triangles), the gas temperature is very uniform. This is due to the effect of grain heating and is consistent with the choice of the interface as mentioned before. As we go outwards from the interface, flow velocity increases and cooling due to expansion of the gas becomes important. Then, the temperature decreases very abruptly and reaches a minimum value. In the neighborhood of this minimum temperature point, the density decreases rapidly (see Fig. 3) and, correspondingly, the optical depth for EUV radiation, $\tau_{\rm EUV}$, becomes small. Then, EUV heating becomes effective and the temperature turns to increase rapidly. The temperature at the sonic point (as denoted by the closed circles in Figs. 2 and 3) is high and it is 4×10^3 K in the model (B).

3.2. *Dependence of the mass loss rate on the EUV flux*

As seen from Fig. 4, the mass loss rate increases with the increase of $\varepsilon F_{\rm EUV}$ but is not necessarily proportional to $\varepsilon F_{\rm EUV}$. This non-linear character will be explained as follows. Integrating Eq. (2·16) from the minimum temperature point (denoted by the subscript m) to the sonic point (denoted by s) and using Eqs. (2·17) and (C·3), we obtain an expression for the mass loss rate, i.e.,

$$|\dot{M}_g| = \int_{r_m}^{r_s} \Gamma 4\pi r^2 dr/(H_s - H_m)$$
$$= \int_{r_m}^{r_s} \Gamma 4\pi r^2 dr \Big/ \left[\frac{GM}{r_m} + \frac{5-3\gamma}{4(\gamma-1)}\frac{GM}{r_s} + \frac{\gamma+1}{4}\left(\frac{\Gamma r}{\rho u}\right)_s\right], \qquad (3\cdot1)$$

where the small terms, ${u_m}^2$ and P_m/ρ_m, have been neglected.

As seen in Fig. 2, both r_m and r_s increase with decreasing $F_{\rm EUV}$ but the increase of r_s is much greater. Furthermore, as seen from Fig. 5, the heat source is localized to a nallow region near $r=r_m$ when $F_{\rm EUV}$ is small. Therefore, the numerator in Eq. (3·1) is proportional to $F_{\rm EUV}$ when $F_{\rm EUV}$ is very small. On the other hand, the second and third terms in the denominator of Eq. (3·1) can be neglected because we have $r_m \ll r_s$ and Γ_s is very small. Therefore, we have in the limit of small flux

$$|\dot{M}_g| \propto F_{\rm EUV}\,. \quad (\text{as} \quad F_{\rm EUV}\to 0) \qquad (3\cdot2)$$

That is, the mass loss rate is proportional to the flux only when this is sufficiently small.

On the other hand, if the EUV flux is very large, the third term in the denominator in Eq. (3·1) is dominant and is proportional to ${F_{\rm EUV}}^{2/3}$ (see Appendix C). Since the numerator in Eq. (3·1) may be approximately proportional to

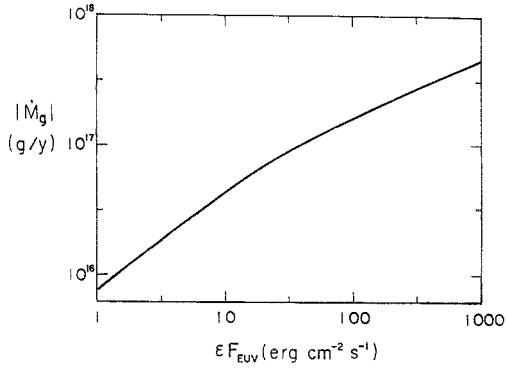

Fig. 4. The mass loss rate $|\dot{M}_g|$ as a function of the EUV flux $\varepsilon F_{\rm EUV}$ for fixed values of $\kappa_g=1\times10^{-4}$ cm^2 g^{-1}, $M/\dot{M}=1\times10^9$ y and $M_g=3.3\times10^{25}$ g.

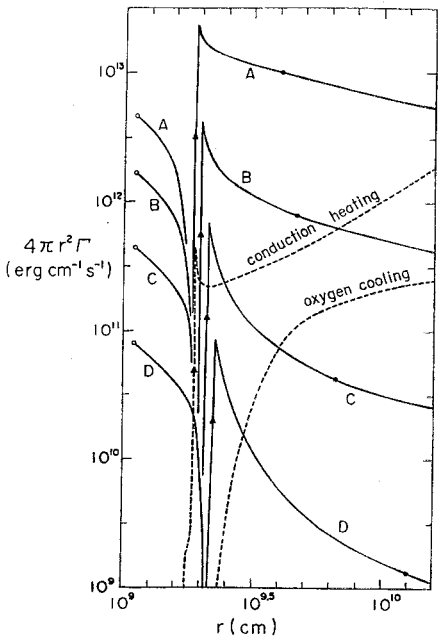

Fig. 5. The distribution of heating rate per unit radial length. The rate of heating by thermal conduction and the rate of cooling by oxygen line emission are also plotted for the model (A).

$F_{\rm EUV}$, we have in the limit of large flux

$$|\dot{M}_g|\propto F_{\rm EUV}{}^{1/3}. \quad (\text{as} \quad F_{\rm EUV}\to\infty) \tag{3·3}$$

This relation means that a major part of absorbed EUV energy is carried away by fluid as its extra thermal and kinetic energies and only a minor part is used to raise the atmosphere against the Earth's gravity. This is more clearly seen from Fig. 6 where H is plotted as a function of r; when $F_{\rm EUV}$ is large, the value of H at $r=r_s$ is much greater than the absolute value of gravitational energy at $r=r_m$.

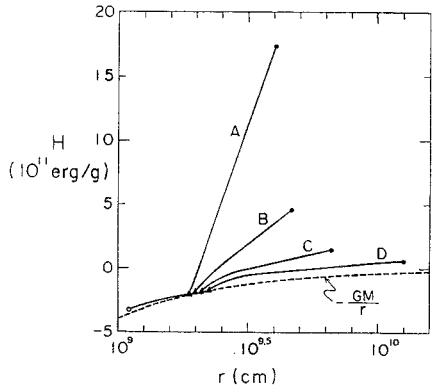

Fig. 6. The distribution of H defined by Eq. (2·17). The gravitational potential of the Earth is also shown for comparison.

3.3. *Dependence on the grain opacity and on the mass accretion rate*

The dependence of the mass loss rate on the grain opacity κ_g will be seen by

comparing the models (B), (E) and (F) in Table I with each other. As κ_g increases, heating of a gas through grains becomes greater and the radius r_m of the minimum temperature point increases (see Fig. 2). Hence, the mass loss rate increases according to Eq. (3·1) but this increase is not large as compared with the increase of κ_g.

On the other hand, the dependence of the mass loss rate on the accretion rate $\dot{M}$ is seen by comparing the models (B) with (G). As seen from Fig. 2, the radius r_m (as well as the radius of the photosphere) decreases with the decrease of $\dot{M}$, so that the mass loss rate decreases slightly according to Eq. (3·1).

3.4. *Examination of assumptions and neglected effects*

(a) Constancy of the luminosity in regions inside the photosphere. For the inner atmosphere we have used static solutions which were obtained by Nakazawa et al.[14] for the case where the energy outflow, L, is constant throughout the atmosphere. Strictly speaking, however, L is not constant in the present problem since a part of L is to be used as energy source for a gas to outflow against the Earth's gravity. That is, the luminosity at the photosphere is decreased by the amount

$$\Delta L = L_b - L_p = \int_{r_b}^{r_p} T\,(ds/dt)\,dM_r\,, \tag{3·4}$$

where the subscripts b and p denote the bottom of the atmosphere and the photosphere, respectively, and d/dt denotes the Lagrangian derivative.

We have estimated ΔL by comparing two models with slightly different atmospheric masses (corresponding to slightly different stages) but with the same values of the other parameters. That is, for a case where $M/\dot{M}=1\times10^9$ y (i.e., $L=1\times10^{23}$ ergs s^{-1}), $M_g=1.6\times10^{26}$ g, $\kappa_g=1\times10^{-4}$ cm^2 g^{-1} and $F_{\mathrm{EUV}}\varepsilon=1\times10^3$ ergs cm^{-2} s^{-1}, we have $\Delta L=1\times10^{21}$ erg s^{-1} which is only 1 percent of the luminosity. Furthermore, as will be seen easily, $\Delta L/L$ decreases as M_g or F_{EUV} decreases. Therefore, the assumption of constant luminosity is a fairly good approximation in our case where $M_g<1.6\times10^{26}$ g and $\varepsilon F_{\mathrm{EUV}}<1\times10^3$ ergs cm^{-2} s^{-1}.

(b) Steady flow. The assumption of steady flow of the outer atmosphere is fairly good, provided that the characteristic time for the change of the atmospheric structure, $t_s\equiv M_g/|\dot{M}_g|$, is much longer than the characteristic flow time, $t_f\equiv H_p/u$ (H_p being the density scale height), at the interface between the inner and the outer atmospheres (note that the value of t_f in the outer atmosphere is greatest at the interface). In all of our models, t_s is much greater than t_f; for example, in the model (H) with $M_g=1\times10^{19}$ g we have $(t_s/t_f)\approx200$ and this ratio increases with M_g. Then, we can conclude that the steady state assumption is justified.

(c) Transfer of the solar EUV radiation. We have assumed that the factor a in Eq. (2·1) is equal to 2. This is true for the density distribution of the

form $\rho \propto r^{-n}$ and $n \gg 1$ (see Appendix B). According to our numerical results, $|\ln \rho / \ln r|$ has a value between 6 and 28 at the EUV photosphere where $\tau_{EUV} = 2/3$. Therefore, the assumption is a good approximation.

(d) Thermal conduction. In Fig. 5, we have plotted the heating rate, Γ_{cond}, due to thermal conduction for the model (A), which indicates that, in regions inside the sonic point, Γ_{cond} is very small compared with Γ, i.e., the total rate of dust- and EUV-heating. Further, in the models (B) to (D), the ratio Γ_{cond}/Γ is smaller than that in the model (A). Therefore, the effect of thermal conduction can be neglected.

(e) Oxygen cooling. The rate of cooling due to forbidden transition between low lying levels of atomic oxygen ($^1S_0$, $^1D_2$, $^3P_0 \cdots$ with $n=1$), excited by $O+H_2$ collision, has been calculated for a case where all of oxygen is assumed to be in the atomic form with the solar abundance. As shown in Fig. 5, this cooling rate, Λ_0, is very small in the model (A) and, further, the ratio Λ_0/Γ in the models (B) to (D) is smaller than that in the model (A), Thus, we can neglect the oxygen cooling entirely.

(f) Dissociation of hydrogen molecules. According to our numerical results, while the gas is flowing from the minimum temperature point to the sonic point, 52 and 17 percent of H_2 molecules are ionized by solar EUV radiation in the models (A) and (B), respectively. Through reactions (A·2) and (A·3) as shown in Appendix A, H is newly produced. Then, cooling due to bound-bound transition of H atoms seems to be important near the sonic point where the temperature is as high as 1.3×10^4 K in the model (A). However, a simple estimate made on an assumption that all of H_2^+ ions become half-and-half H atoms and H^+ ions indicates that the rate of cooling by H atoms is, at most, a half of the rate of EUV heating and, accordingly, the effect of this cooling is not serious.

(g) Effect of the solar wind. If the dynamical pressure, $P+\rho u^2$, of the outflowing gas at the sonic point is greater than that of the solar wind, the flow pattern which has been assumed to be spherically symmetric will not be altered and, accordingly, the effect of the solar wind on the mass loss rate may be neglected. This is the case for all the models in Table I if we adopt the present intensity of the solar wind, as seen from Fig. 7. Furthermore, the above condition is also nearly satisfied even if we consider a case where both the EUV

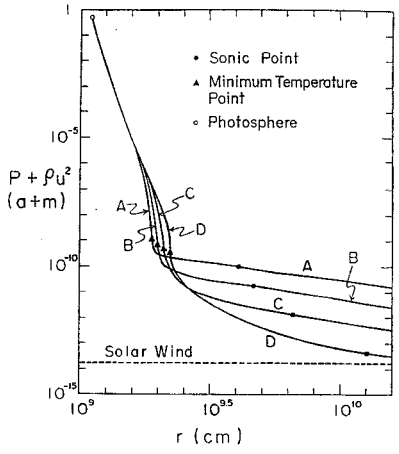

Fig. 7. The distribution of the dynamical pressure, $P+\rho u^2$. The dynamical pressure of the present solar wind is also drawn. The symbols are the same as in Fig. 2.

flux and the wind intensity in the T Tauri stage are greater than their present values by a same factor. Although there is a possibility of much stronger solar wind during the T Tauri stage, the mass loss rate itself would not decreased greatly since, even if the flow pattern is not spherical, the atmospheric gas can escape from the night side of the Earth.

(h) Applicability of hydrodynamics. It is found that, in the inner regions of the sonic point, the molecular mean free path is always smaller than the density scale height if $\varepsilon F_{\rm EUV} \geq 1$ erg cm^{-2} sec^{-1}. Therefore, the application of hydrodynamic equations is correct for all the models.

§ 4. Conclusions and remarks

We have found in the previous section that the mass loss rate depends rather strongly on the EUV flux but very weakly both on the grain opacity and on the mass accretion rate. Now, we look into the dependence of the mass loss rate on the atmospheric mass, M_g, which decreases with time as a result of mass loss itself. This evolutionary change of the mass loss rate is shown in Fig. 8 for the two cases where $F_{\rm EUV}\varepsilon = 1\times10^{2}$ and 1×10^{3} ergs cm^{-2} s^{-1}. As seen from Fig. 1, when M_g is large (e.g., as large as 3×10^{25} g) the radius of the minimum temperature point is much greater than the Earth's radius so that the mass loss rate is large. With decreasing M_g, the minimum temperature point approaches the Earth's surface so that the mass loss rate becomes small and independent of M_g.

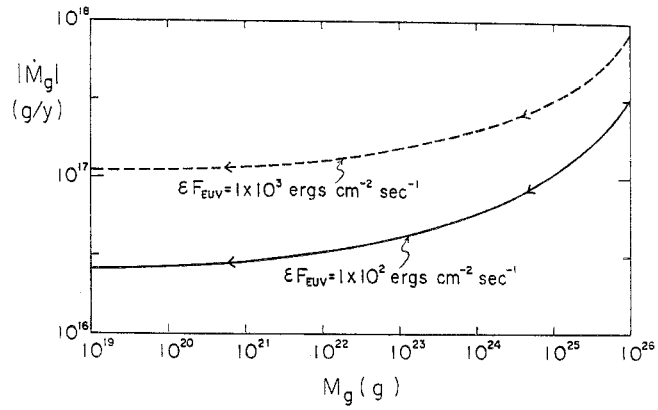

Fig. 8. The mass loss rate $|\dot{M}_g|$ as a function of the atmospheric mass M_g. The solid curve and the dashed curve indicate the cases $F_{\rm EUV}\varepsilon = 100$ and 1000 ergs cm^{-2} sec^{-1}, respectively. The other parameters are fixed to $\kappa_g = 1\times10^{-4}$ cm^2 g^{-1} and $M/\dot{M} = 1\times10^{9}$ y.

In Fig. 9, the total dissipation time of the primordial atmosphere whose initial mass is 1×10^{26} g is plotted as a function of $F_{\rm EUV}\varepsilon$ for a case where $\kappa_g = 1\times10^{-4}$ cm^2 g^{-1} and $M/\dot{M} = 1\times10^{9}$ y. Noticing that $\varepsilon = 0.42$, we conclude from this figure

that if the solar EUV flux during the mass loss stage is greater than 3.3×10^2 ergs cm^{-2} s^{-1}, which is about 2×10^2 times the present solar EUV flux, the atmosphere is dissipated in a period of less than 5×10^8 y, as required from the origin of the present atmosphere.[3] In this case, the rare gases contained in the primordial atmosphere can also be dissipated by the drag of outflowing H_2 molecules, as shown by Sekiya et al.[17] Considering the recent observations of the strong far-UV flux of a T Tauri star, RU Lupi, as mentioned in § 1, we can expect a strong EUV flux, for example, 10^4 times as large as the present one. Thus, the primordial atmosphere may be dissipated within a period of the order of 10^8 y.

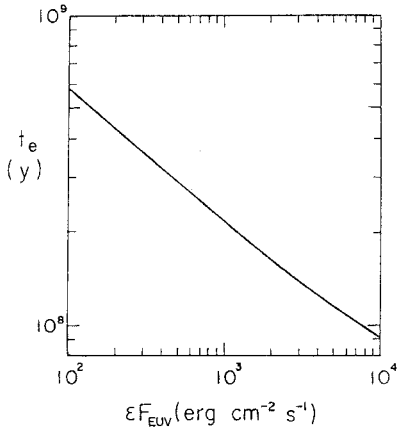

Fig. 9. The total dissipation time, t_e, of the primordial atmosphere as a function of εF_{EUV} for fixed values of $\kappa_g=1\times10^{-4}$ cm^2 g^{-1} and $M/\dot{M}=1\times10^9$ y.

Finally, we discuss briefly the dissipation of the solar nebula itself. Two physical processes have so far been considered for this dissipation. One is the outward transfer of angular momentum due to turbulent viscosity[18] and another is the direct blow-off of the nebula by a strong solar wind.[19] Elmegreen[20] studied a process of angular momentum transfer due to viscosity of turbulent eddies which are generated by a strong solar wind. According to his results, if the solar wind luminosity (i.e., the particle luminosity) during the T Tauri stage is as large as $1L_\odot$ (i.e., about 10^7 times the present solar value), the nebula is dissipated in a period of $10^4/\zeta$ y, where ζ is a coefficient of viscous momentum transfer which lies in the rather wide range, $1/3\sim1/1000$.

Now, by means of a simple energy consideration, we estimate the escape time of the nebula which is blown off by a strong solar wind. If we adopt a distribution of the surface density ρ_s obtained by Kusaka et al.,[4] gravitational binding energy of the whole nebula is given by

$$E=-\int(GM_\odot/2r)\,\rho_s 2\pi r dr=-8\times10^{43}\text{ergs}\,. \tag{4·1}$$

The escape time due to the irradiation of the wind is written as

$$t_e=\frac{-E}{\eta L_W \Omega/4\pi}=3\times10^4\frac{0.1}{\eta}\frac{L_\odot}{L_W}\frac{0.25}{\Omega/4\pi}\text{ y}\,, \tag{4·2}$$

where η is the efficiency of energy transfer from the wind to a surface layer of the nebula, L_W is the solar wind luminosity and Ω is the heliocentric solid angle subtended by the wind-absorbing surface layer of the nebula. We have $\Omega/4\pi\approx0.25$ for the model of Kusaka et al. and probably η is smaller than 0.1. If we put

$\eta=0.1$ in Eq. (4·2), we have a lower limit of the escape time which is just equal to that obtained by Elmegreen as mentioned above. Probably, L_W is of the order of 10^{-2} $L_\odot$ and, then, t_e is of the order of 10^7 y. Anyhow, more precise theoretical treatments as well as more detailed observations of T Tauri stars are needed in order to find a more reliable value of the escape time of the nebula.

Acknowledgements

The authors wish to thank Professor K. Takayanagi and Dr. H. Suzuki for valuable information on some molecular processes. Numerical computations were carried out on a FACOM M-200 at the Data Processing Center of Kyoto University. This work was supported partly by a Grant-in-Aid for Scientific Research of the Ministry of Education, Science and Calture (454047).

Appendix A

——Heating Efficiency of EUV——

The heating efficiency of EUV photons absorbed by H_2 molecules was previously estimated by Henry and McElroy[21] for the Jovian atmosphere and by Glassgold and Langer[22] for interstellar clouds. The former gave the heating efficiency, $\varepsilon=0.86$, on a simple assumption that all the energy except the dissociation energy of H_2 is available for heating, while the latter studied the efficiency more precisely by taking account of various reactions including photon re-emission. Now, we estimate the efficiency considering the existence of excited states of H_3 which were discovered recently by Herzberg.[23]

We consider incident EUV photons with wavelength between 750 and 300 Å, i.e., with energy between 16.5 and 41.3 eV and assume for simplicity that the energy spectrum is flat. The main route of reactions, in which H_2 is finally dissociated into 2H, is given by

$$H_2+\gamma\rightarrow H_2^+ + e^- - 16.5\ \mathrm{eV}, \tag{A·1}$$

$$H_2^+ + H_2 \rightarrow H_3^+ + H + 1.5\ \mathrm{eV}, \tag{A·2}$$

$$H_3^+ + e^- \rightarrow H_3^* \rightarrow H_2 + H + \gamma_1 + 9.5\ \mathrm{eV}. \tag{A·3}$$

The endothermic energy 16.5 eV in (A·1) is a sum of the ionization energy 15.4 eV of H_2 and the vibrational excitation energy 1.1 eV of H_2^+. A part of the emitted electron energy is lost in the excitation and dissociation of H_2, and the remainder is thermalized. The fraction of this thermalized energy was calculated by Glassgold and Langer[22] as a function of the emitted electron energy. Using their results, we find that for the flat EUV spectrum, as assumed above, the average of the thermalized energy per one EUV photon is 5.9 eV (c.f., the average energy of emitted electrons is 12.4 eV).

Now, after the discovery of H_3^* by Herzberg, it is clear that reaction (A·3) proceeds through the intermediate state H_3^* and, consequently, the photon γ_1 is emitted. Since the energy of this photon is not known yet, we assume that the photon carries away a half of the total energy release, 9.5 eV. Then, through reactions (A·2) and (A·3), 6.2 eV is thermalized. Thus, noticing that the average energy of an incident EUV photon is 28.9 eV, we find that the heating efficiency, ε, is $(6.2+5.9)/28.9=0.42$.

Appendix B

——Optical Relations for Power-Law Density Distribution——

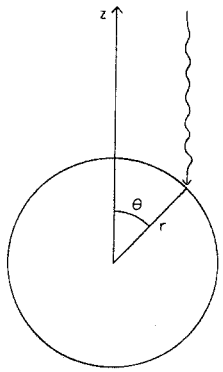

Fig. 10. Geometry of penetration of the solar radiation.
The z axis is directed to the sun.

We consider a case where density distribution is spherically symmetric and is proportional to r^{-n} (n being a constant). If incident photon rays are parallel to the z-axis (see Fig. 10), the optical depth at a point (r, θ, ϕ) in the spherical coordinates is given by

$$\tau(r,\theta)=\int_{r\cos\theta}^{\infty}\frac{\kappa\rho(r)r^n dz}{(z^2+r^2\sin^2\theta)^{n/2}}=\kappa\rho(r)rI_n(\theta)\,, \tag{B·1}$$

where

$$I_n(\theta)=\int_{\cos\theta}^{\infty}\frac{dp}{(p^2+\sin^2\theta)^{n/2}}\,, \tag{B·2}$$

and we have assumed that opacity κ is constant. If n is an integer ($n\geq 2$), we can integrate Eq. (B·2) analytically and we have, for example,

$$I_2=\frac{\theta}{\sin\theta}\,,\quad I_3=\frac{1}{1+\cos\theta}\,,\quad \cdots,\quad I_7=\frac{8+9\cos\theta+3\cos^2\theta}{15(1+\cos\theta)^3}\,,\quad \cdots. \tag{B·3}$$

Furthermore, for $\theta\ll 1$, the denominator in Eq. (B·2) is expanded in a power

series of $(\sin\theta/p)^2$ and we have for a general value of n

$$\tau(r,\theta)=\kappa\rho(r)r\left\{\frac{1}{n-1}+\frac{1}{2(n+1)}\theta^2+O(\theta^4)\right\}. \tag{B·4}$$

It is to be noticed from Eqs. (B·3) and (B·4) that $I_n(\theta)$ takes a minimum value at $\theta=0$.

Now, we consider the average of the heating rate, $F\varepsilon\rho(r)e^{-\tau(r,\theta)}$, taken over a spherical shell with radius r and let it be denoted by $\Gamma(r)$, i.e.,

$$\Gamma(r)=F\varepsilon\rho(r)e^{-\tau(r,0)}\int_0^{\pi}e^{-\tau(r,\theta)+\tau(r,0)}\sin\theta d\theta/2\,. \tag{B·5}$$

In the case $\tau(r,0)\gg1$, the integrand of Eq. (B·5) has a sharp maximum at $\theta=0$ and, then, using Eq. (B·4) we find that the integral is approximated by $1/a\tau(r,0)$ where a is given by

$$a=2(n-1)/(n+1). \tag{B·6}$$

On the other hand, in the case $\tau(r,0)\ll1$, the integral in Eq. (B·5) is nearly equal to unity. Consequently, we obtain Eq. (2·1) as an approximate expression for Eq. (B·5) which can be applied to both of the cases $\tau\gg1$ and $\tau\ll1$.

Appendix C

——Sonic Point for Steady Spherical Flow——

In the presence of heating sources, the equation which determines the sonic point is rather complicated compared with the isothermal and polytropic cases. From Eqs. (2·11) to (2·13), we have

$$\frac{d\ln c}{d\ln r}=\frac{\gamma-1}{c^2-u^2}\left[u^2-\frac{GM}{2r}+(1-\gamma\beta^2)\frac{\Gamma r}{2\rho u}\right] \tag{C·1}$$

and

$$\frac{d\ln u}{d\ln r}=\frac{2}{c^2-u^2}\left(\frac{GM}{2r}-\frac{\gamma-1}{2}\frac{\Gamma r}{\rho u}-c^2\right), \tag{C·2}$$

where c and $\beta(=u/c)$ are the sound velocity and the ratio of the fluid velocity to the sound velocity, respectively. As can be seen easily from the above equations, the sonic point is determined by the conditions

$$c^2=u_s^2=\frac{GM}{2r_s}+\frac{\gamma-1}{2}\left(\frac{\Gamma r}{\rho u}\right)_s, \tag{C·3}$$

where the subscript s denotes the sonic point. If $\Gamma=0$, the above equations reduce to the sonic point condition well-known for a polytropic gas.

Since in our case τ_{EUV} is very small compared with unity at the sonic point, Γ is approximately equal to $\kappa_{EUV}\rho F_{EUV}\varepsilon$. In the limit $F_{EUV}\varepsilon\to\infty$, the first term on the right-hand side of Eq. (C·3) is negligibly small compared with the second term and solving this equation for u_s we obtain

$$u_s\approx\left(\frac{\gamma-1}{2}F_{EUV}\varepsilon\kappa_{EUV}r_s\right)^{1/3}. \quad (\text{as} \quad F_{EUV}\to\infty) \tag{C·4}$$

Therefore, the third term in the denominator in Eq. (3·1) is written in the form,

$$\frac{\gamma+1}{4}\left(\frac{\Gamma r}{\rho u}\right)_s\approx\frac{\gamma+1}{2(\gamma-1)}\left(\frac{\gamma-1}{2}F_{EUV}\varepsilon\kappa_{EUV}r_s\right)^{2/3}. \quad (\text{as} \quad F_{EUV}\to\infty) \tag{C·5}$$

References

1) H. Brown, *The Atmospheres of the Earth and Planets*, ed. G. P. Kuiper (Univ. Chicago Press, 1952), p. 258.
2) F. P. Fanale, Chem. Geol. **8** (1971), 79.
3) Y. Hamano and M. Ozima, *Advance in Earth and Planetary*, ed. E. C. Alexander and M. Ozima (Center for Academic Publ. Japan, 1978), vol. 3, p. 155.
4) T. Kusaka, T. Nakano and C. Hayashi, Prog. Theor. Phys. **44** (1970), 1580.
5) C. Hayashi, K. Nakazawa and I. Adachi, Publ. Astron. Soc. Japan **29** (1977), 163.
6) H. Mizuno, K. Nakazawa and C. Hayashi, Prog. Theor. Phys. **60** (1978), 699.
H. Mizuno, Prog. Theor. Phys. **64** (1980), 544.
7) C. Hayashi, K. Nakazawa and H. Mizuno, Earth Planet Sci. Lett. **43** (1979), 22.
8) H. Mizuno, K. Nakazawa and C. Hayashi, Earth Planet Sci. Lett. **50** (1980), 202.
9) G. F. Gahm, K. Fredga, R. Liseau and D. Dravins, Astron. Astrophys. **73** (1979), L4.
10) S. H. Gross, J. Atmos. Sci. **29** (1972), 214.
11) D. M. Hunten, Icarus **37** (1979), 113.
12) G. P. Horedt, preprint (1980).
13) M. Sekiya, C. Hayashi and K. Nakazawa, in preparation.
14) K. Nakazawa, M. Sekiya, H. Mizuno and C. Hayashi, in preparation.
15) R. D. Hudson, Rev. Geophys. Space Phys. **9** (1971), 305.
16) D. R. Alexander, Astrophys. J. Suppl. **29** (1975), 363.
17) M. Sekiya, K. Nakazawa and C. Hayashi, Earth Planet Sci. Lett. **50** (1980), 197.
18) D. Lynden-Bell and J. E. Pringle, Month. Notices Roy. Astron. Soc. **168** (1974), 603.
19) G. P. Horedt, Astron. Astrophys. **64** (1978), 173.
20) B. G. Elmegreen, Moon Planets **19** (1978), 261.
21) R. J. W. Henry and M. B. McElroy, J. Atmos. Sci. **26** (1969), 912.
22) A. E. Glassgold and W. D. Langer, Astrophys. J. **186** (1973), 859.
23) G. Herzburg, J. Chem. Phys. **70** (1979), 4806.